Bound single-particle states for neutrons from a global spherical optical model

B. Morillon* and P. Romain
Commissariat à l'Énergie Atomique, DAM/DIF/DPTA/SPN, B. P. 12, 91680 Bruyères-le-Châtel, France
(Received 10 February 2006; revised manuscript received 2 May 2006; published 7 July 2006)

The bound single-particle states for neutrons are calculated from our previous global spherical optical model potential containing dispersive terms and a local energy approximation. Reasonably good results are obtained for the single-particle states as well as for the neutron binding energies. This constitutes a further test of our potential.

DOI: 10.1103/PhysRevC.74.014601 PACS number(s): 24.10.Ht, 24.10.Dr, 21.10.Pc

I. INTRODUCTION

Recently we have built a new global optical model potential (OMP) [1] including dispersion relations [2] and the local energy approximation of Perey-Buck [3]. This new global OMP provides a very good description of the total and differential elastic cross sections over a very broad energy domain (1 keV to 200 MeV) for spherical nuclei. Because this OMP is a dispersive OMP with smooth energy dependencies, it is possible to extend it to the negative energy region toward the shell-model potential for $E < 0$ (bound states). This constitutes a further test of our dispersive OMP. Many authors have succeeded in obtaining bound single-particle states for neutrons from different dispersive optical models [4] [5] [6] [7]. In contrast, in this work, those bound states are obtained from a global dispersive OMP.

The paper is structured as follows. In Sec. II, the functional forms of the energy dependencies for the real, imaginary, and spin-orbit potentials are recalled. Some mistakes included in our previous paper are corrected. Dependencies of the depths of the real potentials as well as the dispersive contribution are also shown for positive and negative energies. In Sec. III we present our results for the bound single-particle states energies for ^{208}Pb, ^{90}Zr, and ^{40}Ca, and comparisons with other optical model potentials are given in Sec. IV. Finally, our conclusions are given in Sec. V.

II. OPTICAL MODEL

Our optical model potential can be written as

$$\begin{aligned} U(r,E) = {} & [V_{\rm V}(E) + iW_{\rm V}(E)]f(r,R,a) \\ & - 4a[V_{\rm S}(E) + iW_{\rm S}(E)]\frac{df(r,R,a)}{dr} \\ & - [V_{\rm SO}(E) + iW_{\rm SO}(E)] \\ & \times \left(\frac{h}{m_\pi c}\right)^2 \frac{1}{r}\frac{df(r,R,a)}{dr}\,\mathbf{l}.\boldsymbol{\sigma}, \end{aligned} \tag{1}$$

where $V_{\rm V,S,SO}$ and $W_{\rm V,S,SO}$ are the real and imaginary terms of the volume-central (V), surface-central (S) and spin-orbit (SO) potentials. The volume shape f is a Woods-Saxon form factor.

The volume, surface and spin-orbit shapes share the same geometrical parameters (radius R and diffuseness a). Note also that these parameters are independent of energy. The reduced radius r_0 ($R = r_0 A^{1/3}$) decreases when the nuclear mass A increases, whereas the diffuseness parameter increases with mass.

In the dispersion relations treatment [2], the real V and imaginary W volume potentials are connected by the following expressions:

$$V_{\rm V}(E) = V_{\rm H.F.}(E) + \Delta V_{\rm V}(E), \quad V_{\rm S}(E) = \Delta V_{\rm S}(E), \tag{2}$$

where

$$\Delta V(E) = \frac{P}{\pi}\int_{-\infty}^{+\infty} \frac{W(E')}{E'-E}dE'. \tag{3}$$

As usual, P denotes the principal value of the integral, and $V_{\rm H.F.}(E)$ the Hartree-Fock contribution to the mean field.

A. Imaginary potentials

The energy dependence of the volume and of the spin-orbit imaginary terms is taken to be the form first suggested by Brown and Rho [8]. For the surface imaginary term, we use a Brown-Rho shape modified by an exponential falloff. The parameters of the surface imaginary potential are slightly different from our previous work [1] and give slightly better results. The depth $A_{\rm S}$ of the surface imaginary potential increases with mass as

$$A_{\rm S} = -17 + 0.018\ {\rm A\ (MeV)},$$

whereas the $C_{\rm S}$ and $B_{\rm S}$ parameters are constant:

$$B_{\rm S} = 13\,{\rm MeV}, \quad C_{\rm S} = 0.025\ {\rm MeV}^{-1}.$$

B. Real potentials

We use a local energy approximation for the Hartree-Fock potential adapted from Perey and Buck [3] as explained in Ref. [1]. However, note that there was a mistake in the γ value in our previous paper. The value of γ given in [1] overestimated the right value by a factor of 2 [9]. The true nonlocality range γ decreases slowly with mass:

$$\gamma = 0.1165 - 10^{-4}\ {\rm A\ (fm)}.$$

*Electronic address: benjamin.morillon@cea.fr

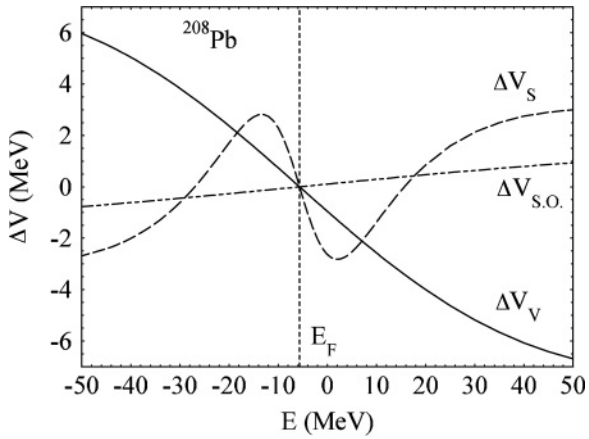

FIG. 1. Energy dependence of the volume (solid curve), surface (long-dashed curve) and spin-orbit (short-dashed curve) dispersive contributions for ^{208}Pb between −50 and 50 MeV.

The real spin-orbit potential is also connected to the imaginary spin-orbit potential by a dispersion relation and has the form given in Ref. [1].

C. Energy dependencies

Because all the energy dependences of the imaginary potential are symmetric about the Fermi energy $E_F(E_F = -[S_n(Z, N) + S_n(Z, N + 1)]/2)$, the dispersive contributions are skew symmetric with respect to E_F. The energy dependencies of the volume, surface and spin orbit dispersive contributions for ^{208}Pb are represented between −50 and 50 MeV in Fig. 1.

To calculate the total volume real potential $(V_{H.F.}(E) + \Delta V_V(E))$, the volume dispersive contribution $\Delta V_V(E)$ is added to the Hartree-Fock potential $V_{H.F.}$. This term $(V_{H.F.})$ is obtained from Eq. (7) of Ref. [1] for positive and negative energy, so that the local energy approximation of Perey-Buck is used to calculate the bound-state properties, too. The total volume real potential and the Hartree-Fock potential are plotted as solid and dashed curves, respectively, in Fig. 2. For large negative energies, $|V_{H.F.}(E) + \Delta V_V(E)|$ is larger than a

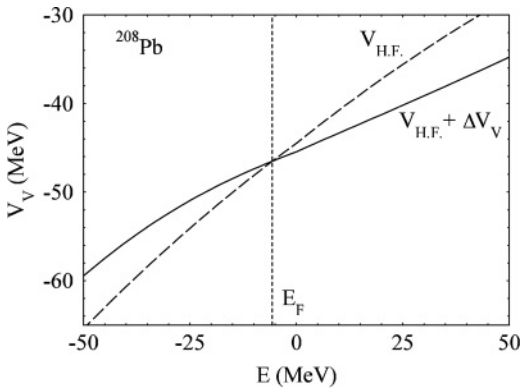

FIG. 2. Depths of volume real potential for ^{208}Pb. The dashed curve gives the variation of the Hartree-Fock potential, and the solid line the total volume potential.

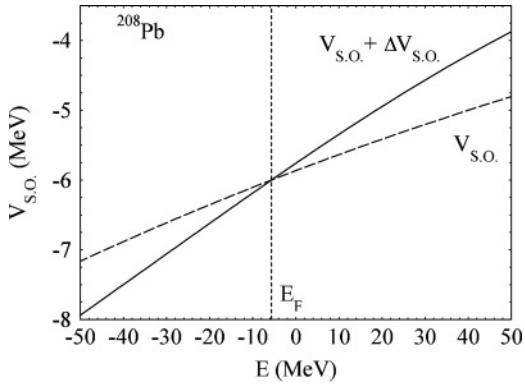

FIG. 3. Depths of spin-orbit real potential for ^{208}Pb. The solid curve gives the variation of the total spin-orbit potential, whereas the dashed curve gives the variation without the dispersion contribution.

simple extrapolation of the volume real potential for negative energy.

The depth of the real spin-orbit potential is represented in Fig. 3 with (solid curve) and without (dashed curve) the dispersion contribution of the imaginary spin-orbit potential.

III. SINGLE-PARTICLE ENERGIES

Our nonlocal, dispersive, and spherical neutron optical model is now specified for positive and negative energy. To calculate the wave functions and the energies of the bound single-particle neutron states, we solve the Schrödinger equation for negative energies with the real potential only (including, of course, the dispersive contributions deduced from the imaginary potentials). For each energy, the Schrödinger equation is solved twice, outward from the origin and inward from 20 fm, until the matching condition of the two solutions is fulfilled. The search of the bound states is now included in the NUCLEON code [1].

At this stage, it is important to note that all the results for the bound single-particle states will be obtained from a potential devoted to scattering problems only. As a matter of fact, the abundant and varied scattering data from positive energies shape the dispersive potential for negative energies. For negatives energies, the Hartree-Fock potential is fixed by the local energy approximation, and all the imaginary potentials are well defined because they are assumed to be symmetric about the Fermi energy. The only doubt resides in the real spin-orbit potential, which is simply extended to negative energies without any proof.

Among the spherical nuclei, experimental values of the neutron single-particle energies are available for ^{208}Pb,^{90} Zr, and ^{40}Ca. (The energies of the various single-particle and hole states for those three nuclei can be found in Refs. [4], [7], and [6], respectively.) The single-particle and hole state energies calculated with the real part of our OMP are shown in Fig. 4 over the heading "M.R." for ^{208}Pb,^{90} Zr, and ^{40}Ca and are compared with the experimental values labeled "Exp.". The general description of single-particle and hole

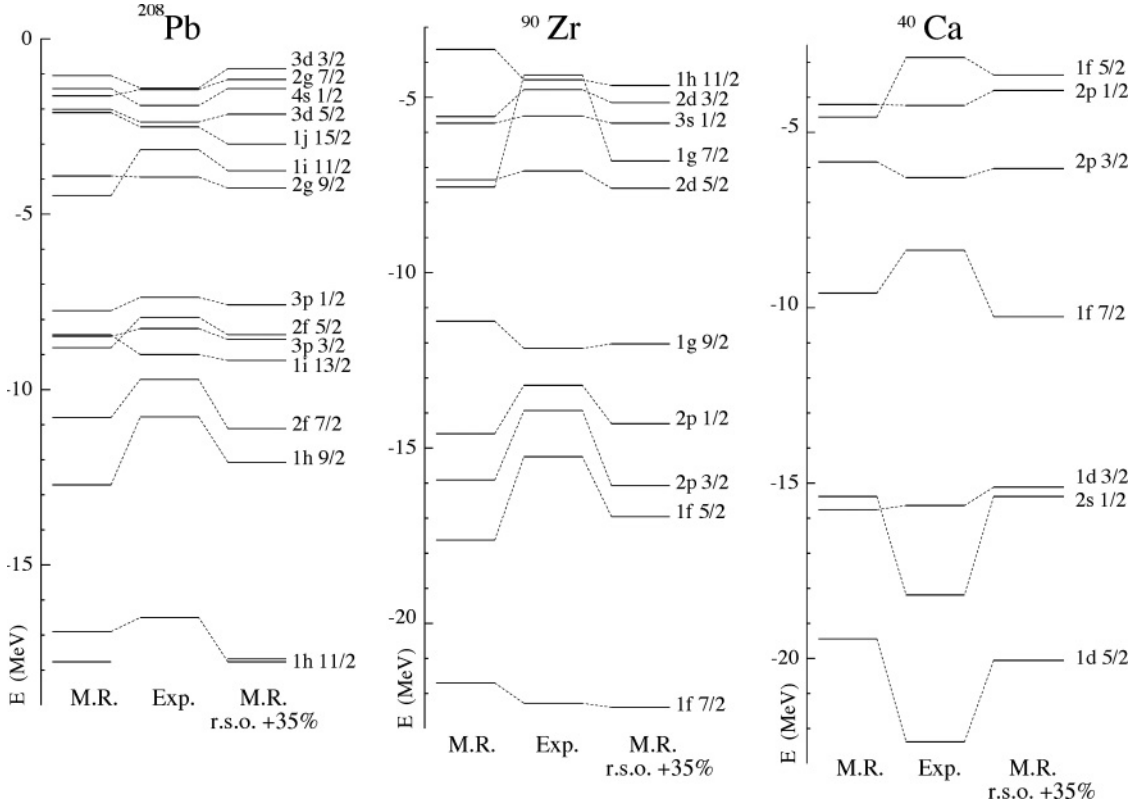

FIG. 4. Neutron single-particle energies in ^{208}Pb, ^{90}Zr, and ^{40}Ca. For each nucleus, the left column displays the values calculated from our potential, the right column those calculated with the real spin orbit increased by 35%, and the central column the experimental values.

states is reasonably good, since all these results are obtained without any change to our original OMP. However, a better agreement is obtained for the ^{208}Pb, where the root-mean-square (r.m.s.) deviation between theory and experiment is 400 keV for particle and 700 keV for hole states as given in Table I. Larger r.m.s. deviations are obtained for ^{90}Zr and ^{40}Ca (cf. Table I). Note that the sequential ordering of the single-particle levels exhibits many inversions. In order to improve the agreement between theory and experiment and because the spin-orbit potential for negative energies is doubtful, this potential has been modified. The results obtained when the real spin-orbit (r.s.o.) potential is increased by 35% are also plotted in Fig. 4 (over the heading "M.R. r.s.o. +35%"), and the r.m.s. deviation between theory and experiment is shown in Table I for every nucleus. The results are lightly better for ^{90}Zr and ^{40}Ca and lightly worse for ^{208}Pb, but the improvement resides in the sequential ordering of the single-particle levels.

TABLE I. Root-mean-square deviation between theory and experiment for particle and hole states with the original M.R. potential and with a 35% increase of the real-spin orbit potential.

Nucleus	M.R.		M.R. r.s.o. +35%	
	Particle	Hole	Particle	Hole
^{208}Pb	400 keV	700 keV	600 keV	900 keV
^{90}Zr	1.7 MeV	1.6 MeV	1.3 MeV	1.3 MeV
^{40}Ca	1.1 MeV	2.3 MeV	1.0 MeV	2.1 MeV

With our shell-model potential, it is easy to obtain the neutron binding energies $S_n(A)$ for spherical nuclei. All we have to do is to calculate the neutron single-particle energies for a nucleus of A nucleons and to locate the shell of the last neutron; the energy of this shell defines the $S_n(A)$ value. From the next upper shell, the neutron binding energy $S_n(A+1)$ is obtained. In Fig. 5 comparisons of the experimental neutron binding energies from Ref. [10] (solid lines) with those calculated with our shell-model potential (long-dashed lines) are shown. The calculations are in good agreement with the data for nuclei between masses 48 and 92 as well as for heavy nuclei. On the other hand, the agreement between theory and experiment is worse for lighter nuclei. The short-dashed lines in Fig. 5 represent the neutron binding energies when the real spin orbit is increased by 35%. No major improvement is obtained by using this modified potential.

IV. COMPARISON WITH OTHER OPTICAL MODEL POTENTIALS

It is interesting to compare our results for the bound-state domain with those obtained from a global but nondispersive OMP. Since the Koning-Delaroche OMP [11] is a non-dispersive OMP and provides good results for scattering

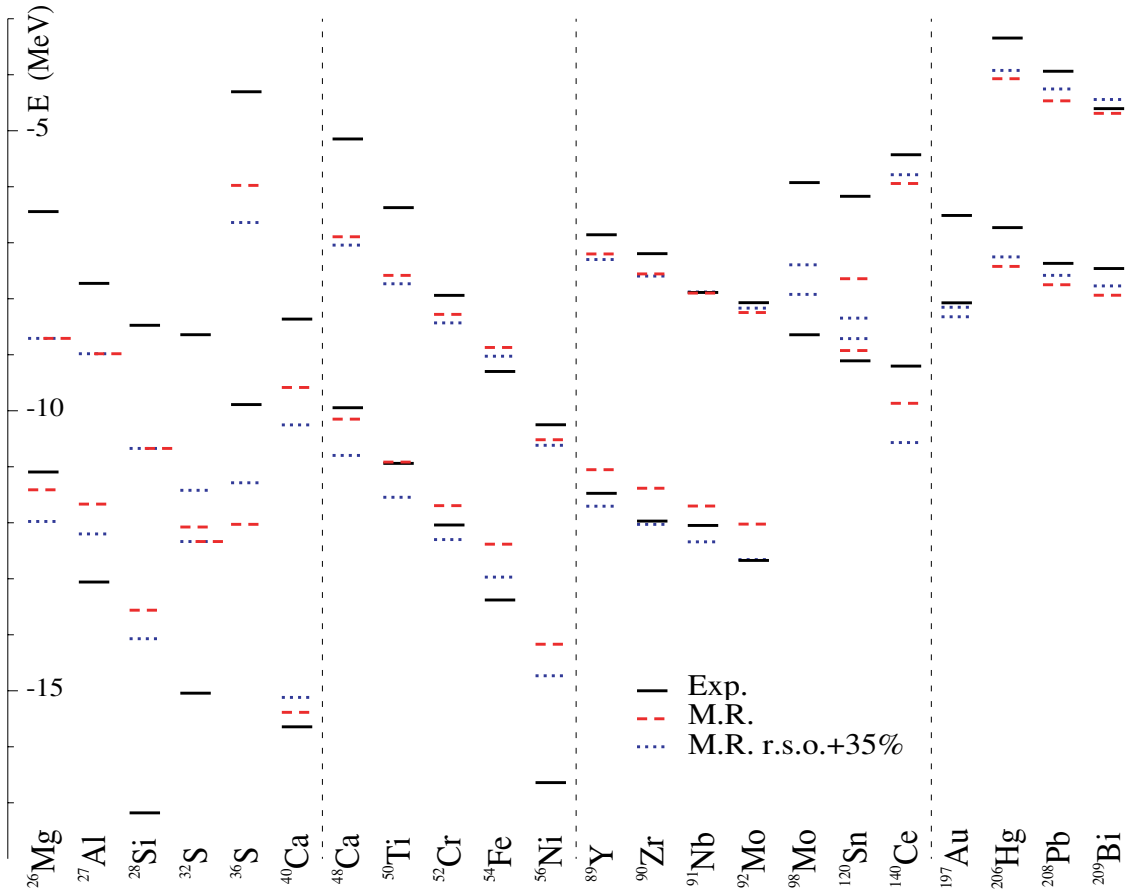

FIG. 5. (Color online) For a given nucleus of A nucleons, the lower and upper solid lines show the experimental neutron binding energies $S_n(A)$ and $S_n(A+1)$, respectively. These values are compared with the binding energies calculated by using the original potential (long-dashed lines) and by using the original potential with the real spin orbit increased by 35% (short-dashed lines).

problems with spherical nuclei, we propose to compare our results with those from this OMP. A comparison with the Bear and Hodgson potential [12], devoted to bound single-particle states, is also attractive because this potential is a simple, physically realistic potential independent of energy for surface states.

The Koning-Delaroche OMP has been defined for positive energy only. We have to extrapolate the real part of the potential to negative energy in order to calculate the bound single-particle neutron states. For that, we use the first order of the tangent equation for $E = 0$ of the real volume depth (we have used the notation of Ref. [11]):

$$V_V(E) = v_1^n \left[1 - v_2^n \left(E - E_f^n\right) + v_3^n \left(E_f^{n^2} - 2E_f^n E\right) + v_4^n \left(E_f^{n^3} - 3E_f^n E\right)\right].$$

The Koning-Delaroche spin-orbit potential is used for negative energy, as we did with our OMP, in order to calculate the bound states.

The depth of the Bear-Hodgson volume potential is written for the neutron surface states as

$$V = V^n \quad \text{for} \quad -15 < E < 0$$

and for the deep states as

$$V = V^n - \beta(E + 15) \quad \text{for} \quad E < -15,$$

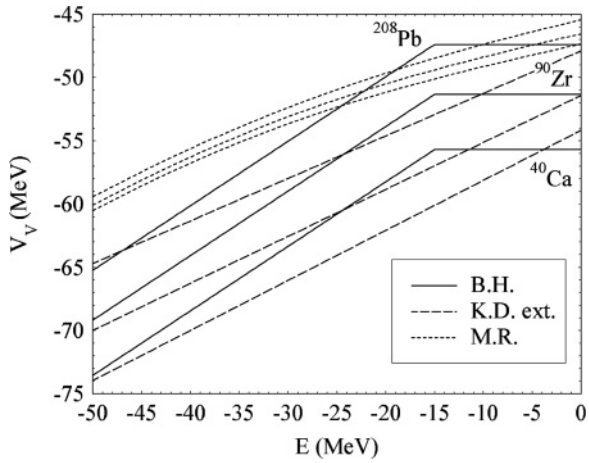

FIG. 6. Energy dependence of the depth of the Bear-Hodgson (solid lines), Koning-Delaroche (long-dashed lines) and Morillon-Romain (short-dashed lines) real volume potentials for ^{208}Pb, ^{90}Zr and ^{40}Ca. For the three potentials, ^{208}Pb is the highest curve, ^{90}Zr, the middle curve, and ^{40}Ca the lowest curve.

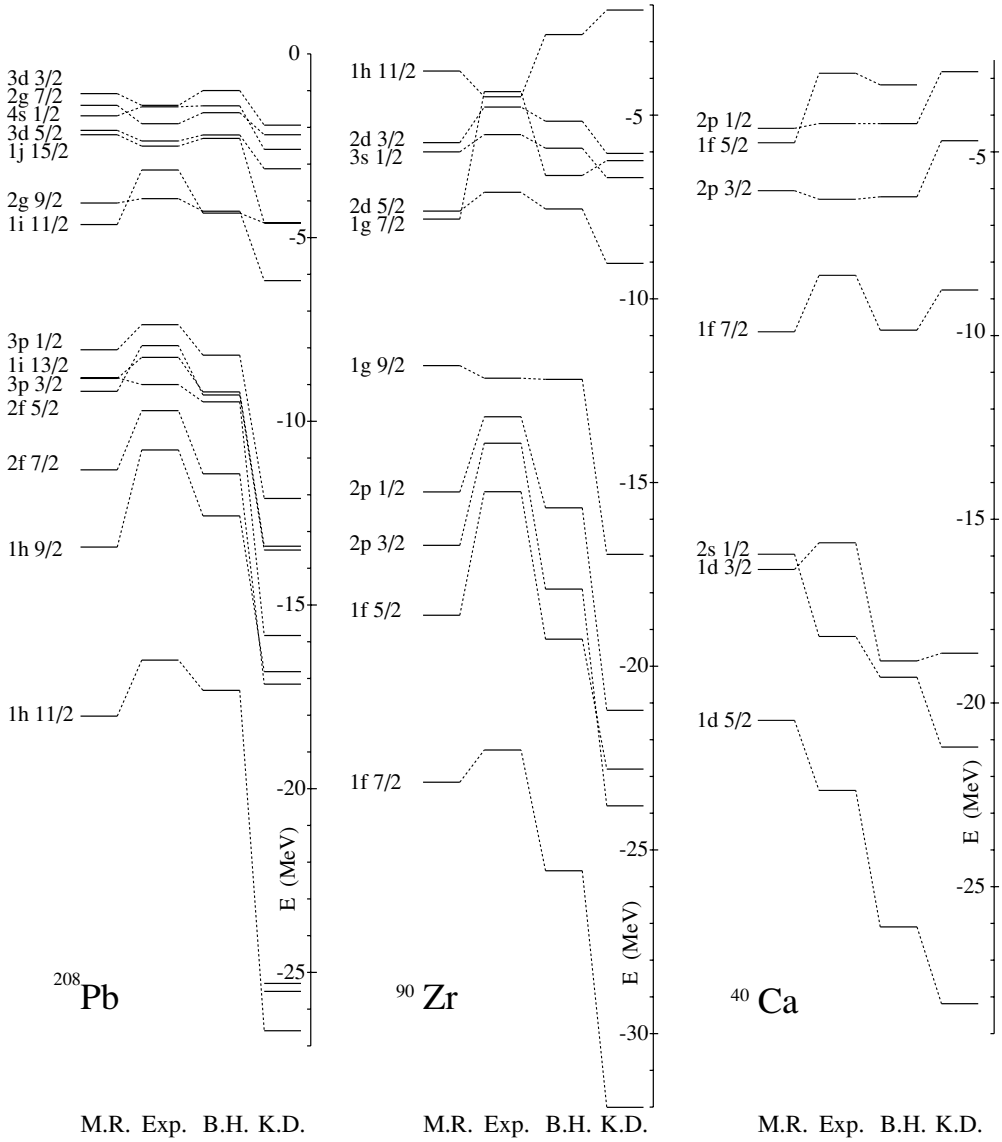

FIG. 7. Neutron single-particle energies in ^{208}Pb, ^{90}Zr, and ^{40}Ca. For each nucleus, the first column displays the values calculated from our potential (M.R.), the third column shows the results obtained with the Bear-Hodgson potential (B.H.), and the last column are those with the extrapolated Koning-Delaroche potential (K.D.). The column labeled "Exp." contains the experimental values.

where the potential V^n is equal to

$$V^n = V_0 - \frac{N-Z}{A} V_1.$$

Bear and Hodgson adopted the average values $V_0 = -55.7$ MeV, $V_1 = -39.3$ MeV, and $\beta = 0.51$ to defined the real volume potential; the depth for the real spin-orbit potential is equal to -7 MeV. The form factor parameters were fixed to the value $r_V = r_{so} = 1.236$ fm, $a_V = 0.62$ fm, and $a_{so} = 0.65$ fm.

Energy dependencies of the depths of the real-volume potential for three nuclei (^{208}Pb, ^{90}Zr, and ^{40}Ca) are shown in Fig. 6. The Bear-Hodgson potential is the solid lines, the extrapolated Koning-Delaroche OMP the long-dashed lines, and the Morillon-Romain OMP the short-dashed lines. Our OMP is seen to give little differences between nuclei as well as small variations from 0 to -50 Mev, incontrast to Bear-Hodgson and the extrapolated Koning-Delaroche potentials.

The single-particle and hole states of ^{208}Pb, ^{90}Zr, and ^{40}Ca predicted with the Morillon-Romain, the Bear-Hodgson and the extrapolated Koning-Delaroche OMP (labelled "M.R.", "B.H" and "K.D.", respectively) are compared with experimental values (over the heading "Exp.") in Fig. 7. The agreement between the single-particle energies calculated with the Bear-Hodgson potential and the experimental values is as good as between our potential and experiment. One surprising result is that both Bear-Hodgson and Morillon-Romain potentials give similar results for the neutron surface states, whereas the energy variation of the real depth is completely different. However, the results obtained with the extrapolated Koning-Delaroche potential are far from the experimental values, and the discrepancy increases for deeper bound states.

Our global dispersive OMP yields results that are better than those obtained from a global nondispersive OMP.

V. CONCLUSIONS

In this work, we have studied the transition between the optical-model and the shell-model potential for our neutron global OMP. Thanks to the dispersion relation and to the local energy approximation, the potentials for negative energies are still defined except for the real spin-orbit term. This OMP, constrained only by diffusion data, is able to provide a reasonably good description of bound single-particle states, even if a modest improvement is obtained with a modified real-spin orbit potential. Moreover, we have shown that the agreement between calculated bound states and experimental values is better when we use a dispersive OMP.

In the future, we plan to construct a global neutron and proton OMP. For this purpose, comparisons between experimental and calculated bound single-particle states for neutrons and protons will lead to a better OMP.

ACKNOWLEDGMENTS

We are very grateful to R. Lazauskas, H. Duarte, and N. Pillet for useful discussions and to E. Bauge for a critical reading of the manuscript.

[1] B. Morillon and P. Romain, Phys. Rev. C **70**, 014601 (2004).
[2] C. Mahaux, H. Ngô, and G. R. Satchler, Nucl. Phys. **A449**, 354 (1986).
[3] F. G. Perey and B. Buck, Nucl. Phys. **32**, 353 (1962).
[4] C. H. Johnson, D. J. Horen, and C. Mahaux, Phys. Rev. C **36**, 2252 (1987).
[5] J. P. Delaroche, Y. Wang, and J. Rapaport, Phys. Rev. C **39**, 391 (1989).
[6] C. Mahaux and R. Sartor, Nucl. Phys. **A528**, 253 (1991).
[7] S. Chiba, P. T. Guenther, A. B. Smith, M. Sugimoto, and R. D. Lawson, Phys. Rev. C **45**, 1260 (1992).
[8] G. E. Brown and M. Rho, Nucl. Phys. **A372**, 397 (1981).
[9] R. Capote, private communication.
[10] G. Audi, A. H. Wapstra, and C. Thibault, Nucl. Phys. **A729**, 337 (2003).
[11] A. J. Koning and J. P. Delaroche, Nucl. Phys. **A713**, 231 (2003).
[12] K. Bear and P. E. Hodgson, J. Phys. G, **4**, L287 (1978).